

# Basin-scale controls on the molybdenum-isotope composition of seawater during Oceanic Anoxic Event 2 (Late Cretaceous)

Alexander J. Dickson<sup>a,\*</sup>, Hugh C. Jenkyns<sup>a</sup>, Donald Porcelli<sup>a</sup>,  
Sander van den Boorn<sup>b</sup>, Erdem Idiz<sup>b</sup>

<sup>a</sup> *Department of Earth Sciences, University of Oxford, South Parks Road, Oxford OX1 3AN, UK*

<sup>b</sup> *Shell Projects and Technology, Kessler Park 1, 2288 GS Rijswijk, The Netherlands*

Received 5 May 2015; accepted in revised form 31 December 2015; available online 1 February 2016

## Abstract

It is well established that the burial of organic carbon in marine sediments increased dramatically at a global scale at the Cenomanian–Turonian boundary (Oceanic Anoxic Event 2: OAE-2, ~94 Myr ago, Late Cretaceous). Many localities containing chemostratigraphic expressions of this event are not, however, enriched in organic carbon, and point to a heterogeneous set of oceanographic and environmental processes operating in different ocean basins. These processes are difficult to reconstruct because of the uneven geographical distribution of sites recording OAE-2, thus limiting our understanding of the causes and palaeoceanographic consequences of the environmental changes that occurred at this time. A new, highly resolved molybdenum-isotope dataset is presented from the Cape Verde Basin (southern proto-North Atlantic Ocean) and a lower resolution record from the Tarfaya Basin, Morocco. The new data reveal periodic oscillations in the Mo-isotope composition of proto-North Atlantic Ocean sediments, from which coupled changes in the dissolved sulphide concentration and Mo inventories of the basin seawater can be inferred. The cyclic variations in sedimentary Mo-isotope compositions can be hypothetically linked to regional changes in the depth of the chemocline, and in the rate of seawater exchange between basinal waters and global seawater. The new data suggest that a global seawater Mo-isotope composition of ~1.2‰ was reached very soon after the onset of OAE-2, implying a rapid expansion of marine deoxygenation coeval with, or slightly preceding, enhanced global rates of organic-carbon burial. During OAE-2, the modelled flux of Mo into anoxic sediments is likely to have been ~60–125 times greater than at the present day, although the spatial extent of anoxia is unlikely to have been greater than 10% of the total seafloor.

© 2016 The Authors. Published by Elsevier Ltd. This is an open access article under the CC BY-NC-ND license (<http://creativecommons.org/licenses/by-nc-nd/4.0/>).

## 1. INTRODUCTION

Oceanic Anoxic Event 2 (OAE-2) was an interval of widespread organic-carbon burial under conditions of expanded marine anoxia (Schlanger and Jenkyns, 1976; Jenkyns, 1980; Arthur et al., 1990). The event took place ~94 Myr ago, and spanned the Cenomanian–Turonian boundary during a period of extreme global warmth in

the mid-Cretaceous (Jenkyns, 2003; Friedrich, 2010; MacLeod et al., 2013). Sediments deposited during OAE-2 have been recognized from a large number of locations, principally on the basis of unusually carbon-rich deposits (black shales) accompanied by a 2–4‰ positive carbon-isotope excursion (CIE) recognized in carbonates (e.g. Jarvis et al., 2006), bulk marine and terrestrial organic matter (Hasegawa, 1997; Tsikos et al., 2004), and specific biomarkers (Kuypers et al., 1999; van Bentum et al., 2012). The total duration of the event, as defined by the CIE, has been estimated from cyclostratigraphy to have

\* Corresponding author. Tel.: +44 1865 272062.

E-mail address: [alex.dickson@earth.ox.ac.uk](mailto:alex.dickson@earth.ox.ac.uk) (A.J. Dickson).

been between ~370 and 890 kyr (Kuypers et al., 2004; Sageman et al., 2006; Voigt et al., 2008; Meyers et al., 2012; Ma et al., 2014; Eldrett et al., 2015).

Oxygen depletion and organic-carbon burial during OAE-2 have been explained by several hypotheses, involving the emplacement of large igneous provinces (Kuroda et al., 2007; Turgeon and Creaser, 2008; Du Vivier et al., 2014), elevated weathering rates (Frijia and Parente, 2008; Blättler et al., 2011; Pogge van Strandmann et al., 2013), the stimulation of marine productivity from a reduction in nutrient limitation (Kuypers et al., 2002; Adams et al., 2010; Monterio et al., 2012) and basin palaeogeography (e.g. Trabucho Alexandre et al., 2010). Whatever the cause, it is clear that OAE-2 represents a period of profound change in Earth's environmental systems. However, the observation that many marine deposits spanning OAE-2, including those of deep-water character, do not contain evidence for pervasive oxygen depletion (Jarvis et al., 2006; Parente et al., 2007; Takashima et al., 2011; Hasegawa et al., 2013; Eldrett et al., 2014) suggests that basin-scale responses to the environmental changes that took place were not uniform and in many locations overrode the global environmental signal of OAE-2. Unfortunately, the comparative lack of well-resolved marine sections from outside the North Atlantic region, in locations that may not necessarily have experienced oxygen-depleted depositional conditions, represents a fundamental limitation to our ability to understand how ocean deoxygenation and carbon burial became extensive at this time.

Stable-isotope variations of elements that have a strong redox dependency and a global seawater residence time greater than the timescale for whole-ocean mixing (2–3 kyr) are useful tools for estimating the extent of seafloor anoxia during past intervals of geological time. Molybdenum, one such element, has a stable oxyanion ( $\text{MoO}_4^{2-}$ ) in seawater and has a residence time >400 kyr (Emerson and Husted, 1991; Miller et al., 2011). In oxic environments, Mo is slowly removed from seawater by adsorption to Fe and Mn oxhydroxides, with preferential removal of the lighter isotopes (Barling and Anbar, 2004; Wasylenki et al., 2008; Goldberg et al., 2009). Under reducing conditions, Mo is reduced to a sulphide species (tetrathiomolybdate,  $\text{MoS}_4^{2-}$ , likely via a series of intermediate oxythiomolybdate species,  $\text{MoO}_x\text{S}_{4-x}^{2-}$ ) (Eriksson and Helz, 2000), and is rapidly removed from seawater, possibly by association with Fe–S particles (Helz et al., 2011), or by adsorption and/or incorporation into organic particles (Algeo and Lyons, 2006; Dahl et al., 2010; Chappaz et al., 2014). This behaviour results in large enrichments of Mo in sediments where  $\text{H}_2\text{S}$  is present only within sediment pore-waters but overlain by oxic or suboxic water masses (henceforth termed ‘anoxic’ settings), and in sediments where  $\text{H}_2\text{S}$  is present in both pore-waters and in overlying seawater (henceforth termed ‘euxinic’) (Crusius et al., 1996; Scott and Lyons, 2012). Such Mo enrichments can cause a reduction of the seawater inventory of dissolved Mo at times when seafloor anoxia and euxinia becomes widespread either at a global (e.g. Scott et al., 2008; Hetzel et al., 2009) or local/basin scale (Algeo and Lyons, 2006). In hydrographically restricted, euxinic depositional

settings, where the rate of Mo removal to sediments (rather than by advection) can exceed its resupply by watermass exchange, the Mo-isotope composition of sediments can be similar to that of global seawater due to near-quantitative removal (Neubert et al., 2008). Since the global seawater Mo-isotope composition records the global balance of the different redox-dependent Mo removal pathways (Poulson-Brucker et al., 2009; Dickson et al., 2014), the isotopic composition of sediments deposited in euxinic marginal basins offers a means for reconstructing past seawater compositions, and consequently the magnitude of past Mo removal fluxes. In present-day marine settings where Mo is converted to sulphide within sediment pore waters, but where the overlying water is not euxinic, the local seawater inventory of Mo is not greatly depleted and sediment Mo-isotope compositions (expressed as  $\delta^{98/95}\text{Mo}$ ) have been observed to be ~0.7–0.9‰ lower than seawater (Poulson et al., 2006; Poulson-Brucker et al., 2012). This difference, which has been attributed to a fractionation between  $\text{MoO}_4^{2-}$  and Mo-sulphides, followed by removal of the latter into sediments, has also been observed in the geological record (Dickson et al., 2014).

In this study, Mo-isotope compositions have been measured from sedimentary deposits at two sites recording OAE-2 (DSDP Site 367, southern North Atlantic basin; S57 core, Tarfaya Basin, Morocco, Fig. 1). The Tarfaya Basin is located on the Moroccan continental margin, where palaeo-water depths are estimated as a few hundred metres (Kuhnt et al., 2005). The Tarfaya Basin was likely influenced by the upwelling of nutrient-enriched waters during OAE-2, as evidenced by periodic variations in the high accumulation rates of organic carbon, thought to be linked to trade-wind location and strength (Kuhnt et al., 1997; Kolonic et al., 2005). Site 367 is located in the Cape Verde Basin at an estimated palaeodepth of ~3700 m. This region of the southern proto-North Atlantic Ocean was characterized by euxinic, poorly ventilated waters during Cenomanian–Turonian times, and was bordered by shallow seaways (Jenkyns, 2010; Trabucho Alexandre et al., 2010; Westermann et al., 2014). The new datasets presented here build on the molybdenum-isotope data presented by Westermann et al. (2014) by revealing periodic fluctuations in the hydrographic state of the southern proto-North Atlantic Ocean during the acme of OAE-2. The new data also constrain the isotopic compositions of different redox-dependent Mo removal pathways, and allow a calculation of the size of the Mo removal fluxes into oxic, anoxic and euxinic sediments during OAE-2.

## 2. METHODS

The new Tarfaya Basin Mo-isotope data were measured from archived samples of drill core S57 (e.g. Tsikos et al., 2004). The Site 367 samples were obtained from the archive half of the core, which was made available to obtain a higher resolution dataset than the severely depleted working half could allow, and to minimize the effects of oxidation on the sediment geochemistry. Samples were selected at 10 cm intervals from the archive core halves of DSDP Site 367A. Trace-element abundances were measured from

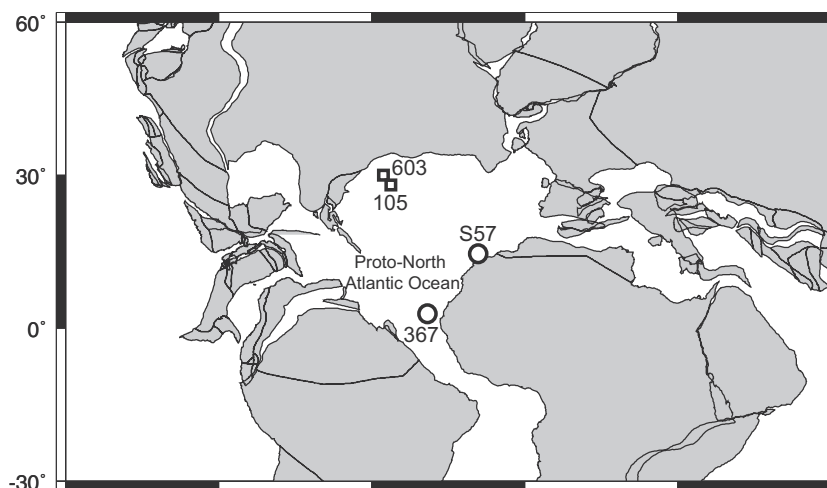


Fig. 1. Study locations. Circles indicate the locations of drill cores analyzed for this study, and squares indicate the location of published data discussed in the text. Map adapted from the ODSN plate tectonic reconstruction service ([www.odsnet.de](http://www.odsnet.de)).

50 mg sample aliquots after digestion on a hotplate using a mixture of concentrated HCl, HNO<sub>3</sub>, and HF acids. Samples were dried and re-dissolved in 2% HNO<sub>3</sub> at dilutions of ~5000 for trace-element analysis and ~500,000 for major-element analysis. Measurements were made using a Perkin–Elmer Inductively Coupled Plasma Mass Spectrometer. Precision and accuracy were monitored with repeat digestions of USGS shale standard SDO-1 and were both better than 10% for Mo, U and Al.

Sample powder aliquots for  $\delta^{13}\text{C}_{\text{org}}$  analysis were decarbonated in 2 M HCl, and rinsed several times in deionized water. Decarbonated powders were weighed into tin capsules and analyzed using a Thermo Flash HT elemental analyzer coupled to a Thermo Finnegan MAT 253 mass spectrometer. Raw  $\delta^{13}\text{C}_{\text{org}}$  values were corrected to the VPDB scale using certified standards (IAEA CH-6 sucrose and NIST 8572 L-glutamic acid) analyzed in the same measurement session. Standard reproducibility during the course of this study was  $\pm 0.06\text{‰}$  for NIST 8572 (1 S.D.,  $n = 15$ ) and  $\pm 0.05\text{‰}$  for IAEA CH-6 (1 S.D.,  $n = 18$ ).

Aliquots of sample powder for Mo-isotope analysis were weighed into Teflon digestion vessels, and an exact mass of a <sup>100</sup>Mo- and <sup>97</sup>Mo-enriched double-spike solution was added to obtain a total Mo spike/sample ratio of ~0.6. The sample powders were digested on a hotplate for 48 h in a 3:1 mixture of concentrated HNO<sub>3</sub> and HCl. Mo was purified from the sample digests using anion-exchange chromatography. This process was based on a method developed by Pearce et al. (2009), but modified with an additional elution step of 0.5 M HF to remove zinc prior to molybdenum elution in 3 M HNO<sub>3</sub>. Stable-isotope measurements were performed on 80 ppb (spike plus sample) solutions using a Nu-Plasma Multi-Collector ICP-MS coupled to a DSN (desolvating nebulizer) sample introduction system. Isotope ratios were calculated offline using a spreadsheet-based deconvolution procedure, and are expressed as  $\delta^{98/95}\text{Mo}$  relative to NIST 3134 (Wen et al., 2010; Greber et al., 2012; Goldberg et al., 2013; Nägler

et al., 2014). The external reproducibility of the method was estimated by processing separate powder aliquots of USGS Devonian Shale standard (SDO-1) through the full chemical purification and analytical procedure and was  $\pm 0.08\text{‰}$  (2 S.D.,  $n = 28$ ). The mean  $\delta^{98/95}\text{Mo}$  composition of SDO-1 was 0.79‰, which is within uncertainty of the value of 0.80‰ estimated by Goldberg et al. (2013).

### 3. RESULTS

#### 3.1. Site 367, Cape Verde Basin

The new high-resolution  $\delta^{13}\text{C}_{\text{org}}$  stratigraphy for Site 367 reveals a +6‰ excursion beginning at 642.05 mbsf (metres below sea floor), with a ~3.5‰ reversal between 641.14 and 640.11 mbsf (Fig. 2 and Table 1).  $\delta^{13}\text{C}_{\text{org}}$  then remains relatively constant above 640.11 mbsf, in an interval that can be correlated to the ‘plateau interval’ of C-isotope values observed at other OAE-2 localities (Tsikos et al., 2004). Mo abundances at Site 367 are elevated above a typical upper crustal concentration of ~1 ppm (Rudnick and Gao, 2003) throughout the study section. Mo-enrichment factors ( $\text{Mo}_{\text{EF}} = [\text{Mo}/\text{Al}]_{\text{sample}}/[\text{Mo}/\text{Al}]_{\text{crust}}$ ) range from ~20 to 4200 with a mean of ~350 (Figs. 2 and 3). U-enrichment factors ( $\text{U}_{\text{EF}}$ ) are similarly elevated relative to an upper crustal concentration of ~2.7 ppm (Rudnick and Gao, 2003), and range from ~1 to 340 with a mean of ~30. The ratio between  $\text{Mo}_{\text{EF}}$  and  $\text{U}_{\text{EF}}$  is approximately 2–10 times higher than the present-day sea-water Mo/U molar ratio of ~7.7 (Algeo and Tribouillard, 2009), confirming that Site 367 was continually overlain by euxinic water masses, in accord with biomarker evidence suggesting that H<sub>2</sub>S extended into the photic zone (Pancost et al., 2004; Sinninghe Damsté and Koster, 1998; Sinninghe Damsté et al., 2008) and the absence of benthic fossils in the core (Čeppek, 1978). The  $\text{Mo}_{\text{EF}}\text{--}\text{U}_{\text{EF}}$  relationship also suggests the presence of an Fe–Mn ‘shuttle’ of particle scavenging of Mo but not U (Algeo and Tribouillard, 2009), which

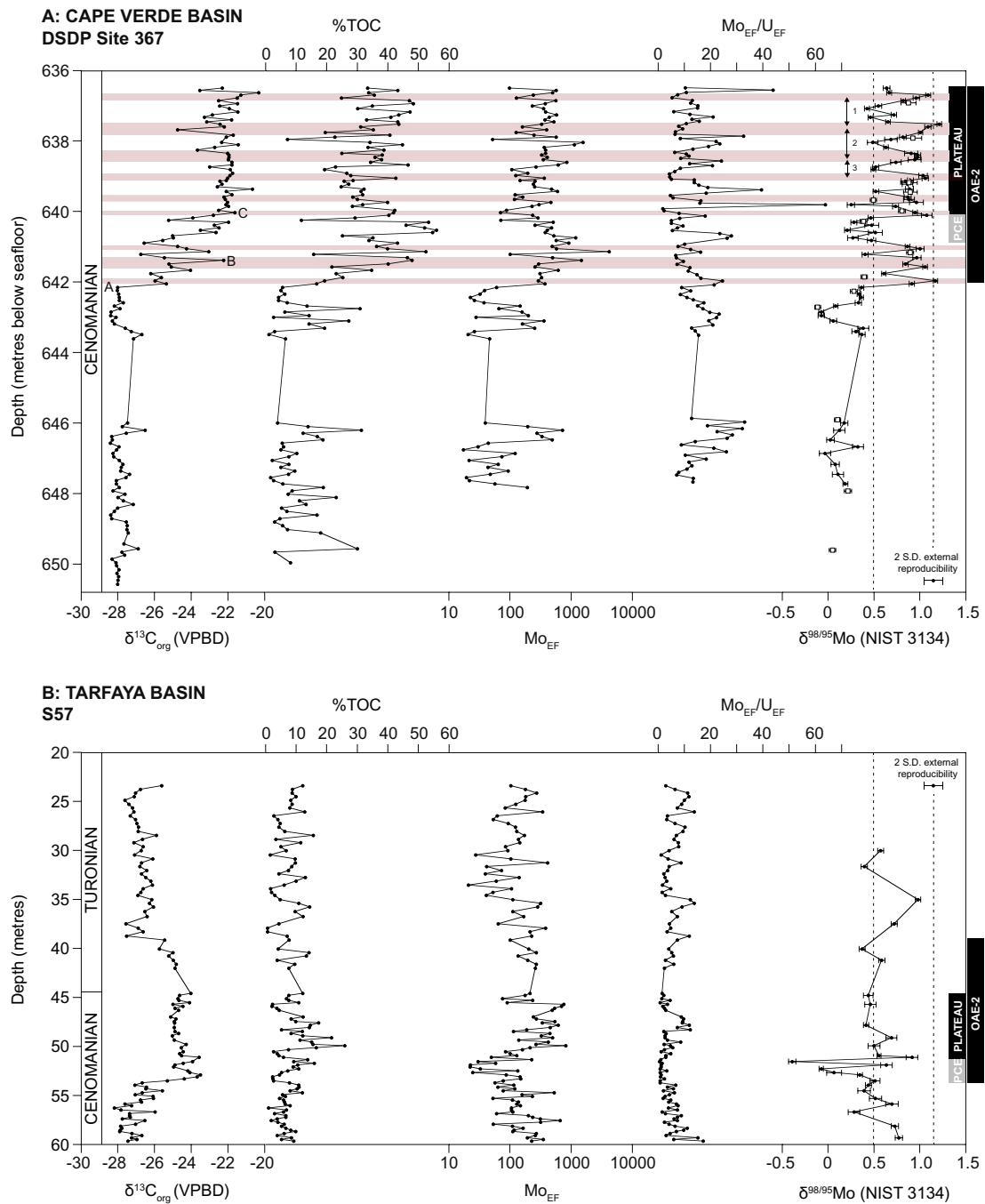


Fig. 2. Stratigraphic data sets from (A) DSDP Site 367, Cape Verde Basin; (B) Research core S57, Tarfaya Basin. Organic-carbon isotopes, percent total organic carbon, Mo enrichment factors, and Mo isotopes are shown for each location. Carbon-isotope and trace-element data for core S57 are from Tsikos et al. (2004) and Kolonic et al. (2005), respectively. The CIE ‘plateau’ interval of relatively constant peak positive values during OAE-2 (c.f. Tsikos et al., 2004) is indicated by a black box for each site. Open squares are the Mo-isotope data from Westermann et al. (2014), which have been re-normalized to NIST 3134 by subtracting 0.26‰ (Goldberg et al., 2013). Note that these data were measured from the working half of Site 367, where sample movement in the core barrel is likely to have affected the exact sample placement with respect to samples from the archive-half analyzed here. PCE: Plenus Cold Event. Letters A, B and C indicate carbon-isotope tie-points used for sedimentation rate estimates discussed in the text. Peaks in  $\delta^{98/95}\text{Mo}$  that correlate to peaks in  $\text{Mo}_{\text{EF}}/\text{U}_{\text{EF}}$  during the CIE plateau interval of OAE-2 are highlighted with grey bars.

would require the presence of ventilated surface waters separated from deeper parts of the basin by a strong chemocline.

Pre-OAE-2  $\delta^{98/95}\text{Mo}$  values at Site 367 fall in the range 0.03–0.38‰, with a small excursion to −0.07‰ at 642.95 and 642.85 mbsf.  $\delta^{98/95}\text{Mo}$  values become higher at the

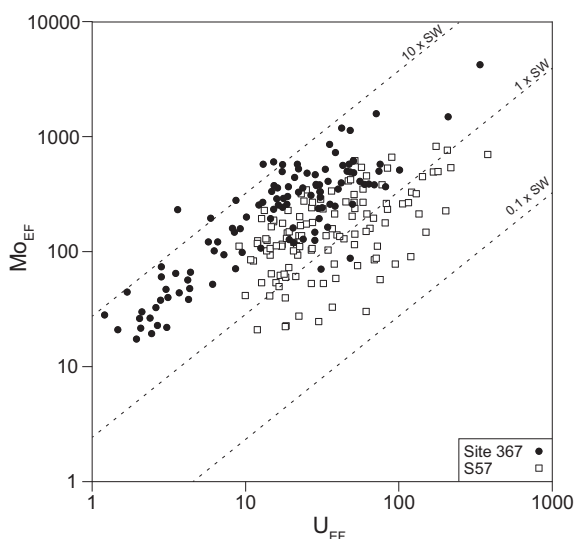


Fig. 3.  $\text{Mo}_{\text{EF}}$  versus  $\text{U}_{\text{EF}}$  for Site 367 and core S57. Dashed lines indicate the present-day seawater  $\text{Mo}_{\text{EF}}/\text{U}_{\text{EF}}$  molar ratio ( $\sim 7.7$ ), converted to a sedimentary abundance ratio of 3.1.

onset of the CIE (642.05 mbsf), reaching a maximum of 1.2‰ (Fig. 2). The subsequent interval of elevated  $\delta^{98/95}\text{Mo}$  is interrupted by a transient excursion to lower values (down to 0.21‰) between 640.99 and 640.18 mbsf. The main ‘plateau’ phase of the OAE-2 CIE at Site 367 is characterized by several oscillations in  $\delta^{98/95}\text{Mo}$  between an average maximum of  $\sim 1.10\text{‰}$  and an average minimum of  $\sim 0.50\text{‰}$  (shaded bands, Fig. 2). Intervals of elevated  $\delta^{98/95}\text{Mo}$  within these oscillations do not show a clear correlation with absolute Mo concentrations, but do correlate with elevated  $\text{Mo}_{\text{EF}}/\text{U}_{\text{EF}}$ .

### 3.2. S57, Tarfaya Basin

$\text{Mo}_{\text{EF}}$  in core S57 fall in the range  $\sim 20$ –820 and average  $\sim 200$  (Figs. 2 and 3 and Table 2).  $\text{U}_{\text{EF}}$  range from  $\sim 10$  to 380 and average  $\sim 50$ . Although biomarkers indicative of photic-zone euxinia occur in sediments deposited throughout the CIE in core S57 (Kolonic et al., 2005), the presence of bioturbated carbonate-enriched horizons, with occurrences of benthic foraminifera (Kuhnt et al., 2005; Kolonic et al., 2005) indicates occasional ventilation of the basin floor, with the chemocline deepening into sediment pore waters. These sedimentary features, which imply that transient re-oxygenation events affected the basin seafloor, are not observed at Site 367. The ratio between  $\text{Mo}_{\text{EF}}$  and  $\text{U}_{\text{EF}}$  spans the present-day seawater Mo/U ratio, reflecting a marginal basin environment that did not experience hydrographic restriction as severely as did Site 367, and which fluctuated between euxinic and suboxic seafloor conditions.

$\delta^{98/95}\text{Mo}$  values in core S57 range from  $-0.40$  to  $1.00\text{‰}$ , and do not exhibit any clear stratigraphic trend with respect to the CIE (as measured by Tsikos et al., 2004) (Fig. 2). During the plateau interval of the CIE,  $\delta^{98/95}\text{Mo}$  values remain approximately constant, with a mean of 0.50

$\pm 0.20\text{‰}$ , which is within uncertainty of the lowest values in the CIE plateau interval at Site 367 (Fig. 2).

## 4. DISCUSSION

### 4.1. Origin of the Mo-isotope cycles in Site 367

The two principal observations stemming from the two Mo-isotope datasets in Fig. 2 are: (i) Despite the extremely TOC-enriched, laminated appearance of the deposits at Site 367, sediment  $\delta^{98/95}\text{Mo}$  is not constant during the plateau phase of OAE-2, but instead fluctuates in an apparently periodic manner with a consistent amplitude of  $\sim 0.65\text{‰}$ . Increases in  $\delta^{98/95}\text{Mo}$  during these fluctuations are accompanied by decreases in the  $\text{Mo}_{\text{EF}}/\text{U}_{\text{EF}}$  ratio. (ii) Sediment  $\delta^{98/95}\text{Mo}$  values from the plateau interval of OAE-2 in core S57 closely parallel the lower bound of the Site 367  $\delta^{98/95}\text{Mo}$  compositions, but do not exhibit any clear excursions to higher values. Three different geochemical models may be put forward as a framework to interpret these observations.

The first model (model ‘A,’ Fig. 4a) is that the sediment  $\delta^{98/95}\text{Mo}$  fluctuations at Site 367 record changes in the  $\delta^{98/95}\text{Mo}$  composition of proto-North Atlantic basin seawater, which in turn is coupled to changes in the global seawater  $\delta^{98/95}\text{Mo}$ . This palaeoceanographic model, which was first proposed by Pearce et al. (2008) for similar cyclic variations in  $\delta^{98/95}\text{Mo}$  in the Yorkshire Basin during the early Toarcian OAE, would require that the global inventory (and therefore residence time) of dissolved Mo was reduced sufficiently for short-duration changes in the balance of input and (redox-dependent) output fluxes to be imprinted on the global seawater  $\delta^{98/95}\text{Mo}$  composition. Furthermore, such a model would also require a stable hydrographic connection between the proto-North Atlantic Ocean and the global ocean, and constancy in the redox state (i.e. euxinic) and/or extent of Mo removal from proto-North Atlantic basin seawater throughout the period of fluctuating  $\delta^{98/95}\text{Mo}$ . The latter requirement is essential in order to eliminate the possibility that Mo-sulphide speciation at different concentrations of dissolved  $\text{H}_2\text{S}$ , (e.g. Tossell, 2005; Neubert et al., 2008; Dahl et al., 2010; Nägler et al., 2011) and/or a change in the magnitude of the dissolved Mo inventory, was responsible for the observed sediment  $\delta^{98/95}\text{Mo}$  fluctuations.

The second model (model ‘B,’ Fig. 4b) is that the sediment  $\delta^{98/95}\text{Mo}$  fluctuations at Site 367 directly record changes in the  $\delta^{98/95}\text{Mo}$  of the overlying proto-North Atlantic basin seawater, which in turn was periodically decoupled from the global seawater  $\delta^{98/95}\text{Mo}$ . This model implies that at times when the dissolved Mo inventory of the proto-North Atlantic Ocean was depleted under the euxinic conditions that prevailed during OAE-2 (Sinninghe Damsté and Koster, 1998; Kuypers et al., 2002, 2004; Pancost et al., 2004; Westermann et al., 2014), the removal of Mo with an isotopic composition lower than the basin seawater into seafloor sediments forced the basin seawater to evolve to higher  $\delta^{98/95}\text{Mo}$  compositions. This phenomenon has been observed to occur in the present-day deep Black Sea ( $>800$  m), where the rapid



removal of dissolved Mo into sediments has led to local dissolved concentrations that are >90% lower than the open ocean (Emerson and Huested, 1991). The  $\delta^{98/95}\text{Mo}$  composition of the deep waters (sub-chemocline) in the Black Sea is correspondingly  $\sim 0.7\text{‰}$  higher than in the open ocean (Näglér et al., 2011). With these considerations in mind, deciding how representative the sediment  $\delta^{98/95}\text{Mo}$  values from Site 367 are of global ocean  $\delta^{98/95}\text{Mo}$  during OAE-2 requires some estimate of the difference between the proto-North Atlantic seawater  $\delta^{98/95}\text{Mo}$  and the global ocean seawater  $\delta^{98/95}\text{Mo}$  during intervals of Mo-depletion. This difference would be expected to change depending on the magnitude of dissolved Mo depletion within the basin, with a higher proportion of Mo removal driving the proto-North Atlantic seawater  $\delta^{98/95}\text{Mo}$  higher than the global ocean. The third model (model 'C,' Fig. 4c) builds on model B by addressing the question of whether the speciation of Mo reaching the sediments remained constant at times when the proportional removal of dissolved Mo from local seawater changed. The fractionation between dissolved Mo and the solid Mo incorporated into the sediments (seawater  $\delta^{98/95}\text{Mo}$  – sediment  $\delta^{98/95}\text{Mo} = \Delta\text{Mo}$ ) might be expected to change, depending

on Mo-sulphide speciation (Eriksson and Helz, 2000; Neubert et al., 2008; Näglér et al., 2011) and/or the addition of Mo incorporated into other phases (e.g. Fe- and Mn-oxides (Siebert et al., 2003; Barling and Anbar, 2004; Wasylenki et al., 2008; Goldberg et al., 2009, 2012)). Observations from the Black Sea (Neubert et al., 2008; Näglér et al., 2011) show that at increasing concentrations of dissolved hydrogen sulphide ( $\text{H}_2\text{S}$ ) in the water column, Mo transitions through a series of oxythiomolybdate species ( $\text{MoO}_x\text{S}_{4-x}^{2-}$ ), with a stable end-member ( $\text{MoS}_4^{2-}$ ) at  $\text{H}_2\text{S}$  concentrations  $>11\text{ }\mu\text{mol/l}$ . Importantly, changes in the speciation of dissolved Mo-sulphides are time-dependent processes, with fast transitions between the intermediate oxythiomolybdate species. However, the conversion of  $\text{MoOS}_3^{2-}$  to  $\text{MoS}_4^{2-}$  takes several months, and requires the persistence of stable dissolved sulphide concentrations exceeding these timescales (Eriksson and Helz, 2000). It is therefore possible to speculate that, during periods when the proto-North Atlantic Ocean Mo inventory was less depleted (model B), a decrease in dissolved  $\text{H}_2\text{S}$  concentrations and a decrease in the residence time of the basin seawater perturbed the speciation of dissolved Mo towards a greater proportion of  $\text{MoOS}_3^{2-}$ . This change

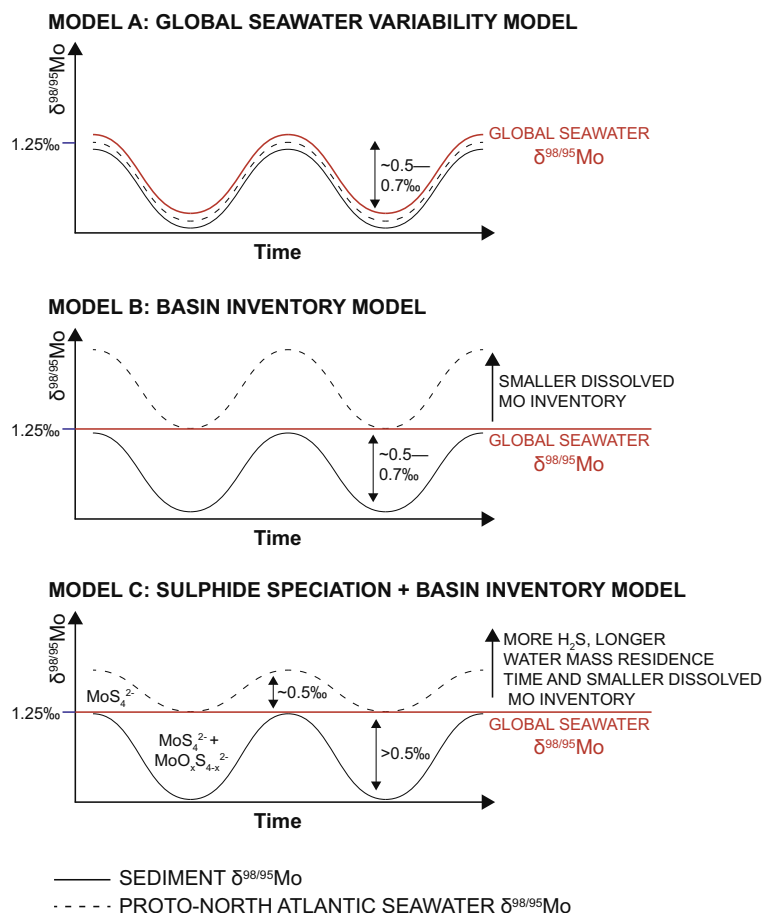


Fig. 4. Models linking basin seawater, global seawater, and sedimentary  $\delta^{98/95}\text{Mo}$  compositions in the proto-North Atlantic Ocean. See text for full discussion.

in speciation would have subtly increased  $\Delta\text{Mo}$ , thereby exaggerating the apparent range of  $\delta^{98/95}\text{Mo}$  in sediments compared to overlying basin seawater.

The key to distinguishing between models A, B and C is to establish whether the hydrographic and redox state of the proto-North Atlantic Ocean fluctuated during OAE-2 (thus favouring a local origin for the Mo-isotope cycles, models B and C), or whether it remained constant throughout the Mo-isotope cycles (thus favouring a global origin, model A). Two indices from Site 367,  $\text{Mo}_{\text{EF}}/\text{U}_{\text{EF}}$  and  $\text{Mo}/\text{TOC}$ , can be explored to distinguish between these two options. In Fig. 2, the ratio between  $\text{Mo}_{\text{EF}}$  and  $\text{U}_{\text{EF}}$  clearly oscillates to higher values in tandem with lower  $\delta^{98/95}\text{Mo}$ . Higher  $\text{Mo}_{\text{EF}}/\text{U}_{\text{EF}}$  could indicate the faster removal of Mo compared to U locally into sediments, which could either reflect enhanced Fe/Mn-shuttling of Mo, but not U, from above the chemocline (e.g. *Algeo and Tribouillard, 2009*), or a higher concentration of dissolved sulphide in the water column that would favour more complete removal of dissolved Mo into the underlying sediments (e.g. *Tribouillard et al., 2006*). Both of these processes would indicate instability in the basin hydrography, and their correlation with Mo-isotope cycles would thus favour a local origin for the isotopic variations. However, the sediment  $\text{Mo}_{\text{EF}}/\text{U}_{\text{EF}}$  ratio could alternatively be caused by changes in the seawater concentrations of the respective elements, due to their differing redox sensitivities and global seawater residence times (*Emerson and Huested, 1991*). If the decreases in  $\delta^{98/95}\text{Mo}$  during each Mo-isotope cycle did indeed record a short-term increase in global ocean anoxia and euxinia, then the more efficient removal of Mo from seawater compared to U under (globally) more sulphidic conditions would be expected to drive residual seawater Mo/U lower, which is opposite to the pattern recorded in Fig. 3. In summary, the phase relationship between  $\text{Mo}_{\text{EF}}/\text{U}_{\text{EF}}$  and  $\delta^{98/95}\text{Mo}$  cycles in Site 367 is more consistent with models B and C, rather than with model A.

The inference from the  $\text{Mo}_{\text{EF}}/\text{U}_{\text{EF}}$  data that basin-scale redox controls are more likely to have driven the Mo-isotope cycles at Site 367 are supported by a second line of evidence based on Mo/TOC ratios. Since Mo and TOC are both enriched in euxinic environments, any change in the Mo/TOC ratio should qualitatively record variability in the dissolved Mo inventory (*Algeo and Lyons, 2006*). Fig. 5a shows the relationship between  $\delta^{98/95}\text{Mo}$  and Mo/TOC for Site 367. Despite exhibiting a degree of scatter, the inverse correlation between the two parameters indicates a control on sediment  $\delta^{98/95}\text{Mo}$  by the dissolved Mo inventory, with lower Mo/TOC ratios corresponding to higher  $\delta^{98/95}\text{Mo}$  values in the CIE plateau interval of OAE-2 (black symbols in Fig. 5a). If the  $\delta^{98/95}\text{Mo}$  cycles were being controlled by the global extent of seafloor anoxia and euxinia, lower sediment Mo-isotope compositions should correspond to lower Mo/TOC ratios (i.e. a smaller global seawater Mo inventory). The fact that the relationship in Fig. 5 is the opposite strongly suggests that the cyclic changes in  $\delta^{98/95}\text{Mo}$  during OAE-2 are instead driven by changes in the basin-scale inventory of Mo. This line of evidence therefore also clearly favours either model B or C as a more likely mechanism

governing Mo-isotope cycles in the deep Cape Verde Basin sediments.

Assuming a depth of water overlying Site 367 of  $\sim 3700$  m (*Lancelot, 1977*), an average sediment Mo concentration of  $\sim 115$  ppm, a sediment bulk density of  $\sim 1.8$  g/cm<sup>3</sup>, a sedimentation rate of  $\sim 1$  cm/kyr, and a present-day Mo global seawater concentration of 105 nmol/kg (*Emerson and Huested, 1991; Miller et al., 2011*) for the proto-North Atlantic Ocean, it would take in excess of 22,000 years for Mo in the overlying water column to be removed into underlying sediments during OAE-2. Alternatively, if the global seawater dissolved Mo concentration were  $\sim 5$ – $10\%$  of its present-day value (i.e.  $\sim 5$ – $10$  nmol/kg), the overlying water column would become depleted in dissolved Mo in only  $\sim 2$  kyrs, which is less than the mixing time of the modern ocean. Such an estimate is consistent with the interpretation of the Mo-isotope and Mo/TOC data from Site 367, and with estimates of global trace-metal drawdown during OAE-2 (*Hetzel et al., 2009; Owens et al., 2013*).

The Mo-isotope data from Tarfaya further support the inferences drawn from Site 367. Although biomarkers for photic-zone euxinia are present during the CIE ‘plateau interval’ of OAE-2 in core S57, (*Kolonic et al., 2005*), and Fe-speciation indicators also indicate euxinic conditions for part of the S57 sedimentary succession (*Poulton et al., 2015*), the range of evidence for bottom-water re-ventilation events in the Tarfaya Basin (above) suggest that it is unlikely that the residence time of seawater in the basin was ever sufficiently high to enable quantitative ( $>90\%$ ) Mo drawdown into the sediments. Under these circumstances, the  $\Delta\text{Mo}$  in the Tarfaya Basin would have been constantly  $>0.5\%$ , and likely closer to the  $\sim 0.7\%$  difference observed between the  $\delta^{98/95}\text{Mo}$  of modern seawater, and sulphidic sediments, at the present day (*Poulson et al., 2006; Poulson-Brucker et al., 2009*). In this sense, the similarity in Mo-isotope compositions at Tarfaya and the lower bound of the Site 367 Mo-isotope cycles supports the idea that these values ( $\sim 0.50\%$ ) record the sulphide-fractionated values from a seawater composition of  $\sim 1.20\%$ . Although the possibility does remain that Mo-isotope excursions in the Tarfaya Basin might be masked by the comparatively low resolution of the data during the OAE-2 interval, it is noteworthy that other locations that experienced anoxia and/or episodic euxinia, but not hydrographic restriction, during the acme of OAE-2 (Furlo and Contessa, Italy, and ODP Site 1276, Newfoundland Basin) also have maximum  $\delta^{98/95}\text{Mo}$  compositions of  $\sim 0.4$ – $0.5\%$  (*Westermann et al., 2014*; renormalized to NIST 3134), which are similar to Tarfaya.

## 4.2. Regional significance of proto-North Atlantic Ocean redox fluctuations

A direct proxy for dissolved H<sub>2</sub>S concentrations is not currently available, but changes in the depth of the chemocline and redox state of proto-North Atlantic deposits spanning OAE-2 have previously been identified from sites located in the Newfoundland Basin (IODP Site 1407; Shipboard Scientific Party, 2012) and DSDP Sites 105

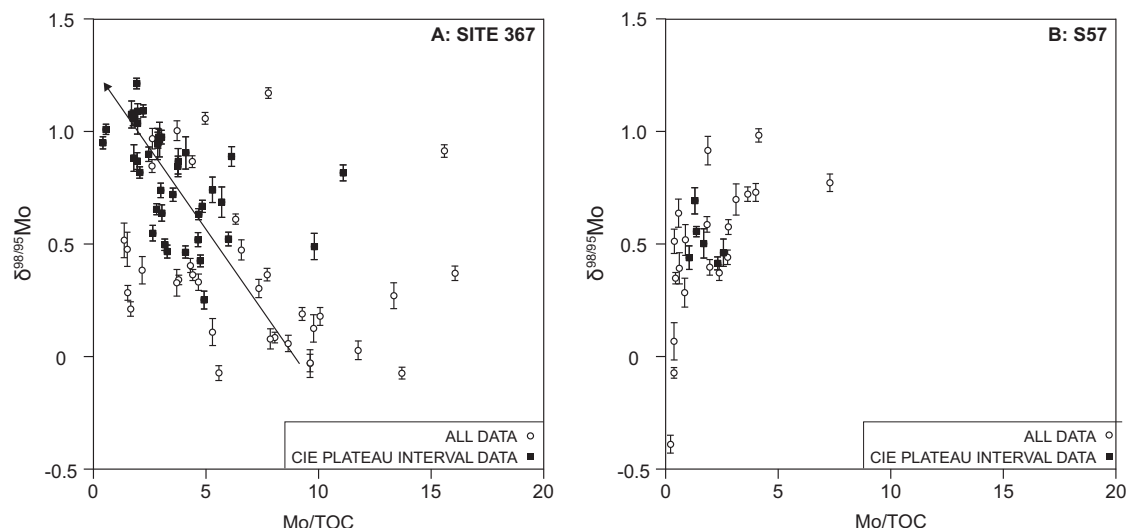


Fig. 5. (A) Plot of Mo-isotope compositions versus Mo abundances normalized to total organic carbon for Site 367. Data from the CIE 'plateau' interval of OAE-2 are represented by solid circles. The arrow indicates the trend in the data towards a  $\delta^{98/95}\text{Mo}$  intercept of  $\sim 1.20\text{‰}$  for a Mo/TOC approaching 0. (B) Plot of Mo-isotope compositions versus Mo abundances normalized to total organic carbon for Tarfaya Basin core S57.

and 603 in the northern proto-North Atlantic (Herbin et al., 1987; Kuypers et al., 2004). At Sites 105 and 603, green marl–black shale alternations throughout the plateau interval of OAE-2 were attributed to fluctuations in productivity and consequently in seafloor redox and the efficiency of organic-carbon burial (Kuypers et al., 2004). Importantly, these changes in productivity were paced by orbital cycles, argued initially to be precession-paced, and more recently argued to be paced by orbital obliquity (Meyers et al., 2012). The association of the marl–shale couplets at Sites 105 and 603 with changes in the abundance of the biomarker isorenieratene (Kuypers et al., 2004) suggests that the productivity changes were accompanied by, and perhaps drove, changes in the depth of the chemocline separating euxinic from non-euxinic seawater in the basin.

The timing and duration of the  $\delta^{98/95}\text{Mo}$  fluctuations at Site 367 can help to demonstrate whether they are related to similar forcing factors as the sedimentary cycles observed in the more northerly Atlantic Ocean cores. The top of the CIE is missing at Site 367, and poor microfossil preservation limits the potential to establish biostratigraphic constraints on how much time is recorded in the sedimentary succession (Čeppek, 1978). Nonetheless, the smooth oscillations in the  $\delta^{98/95}\text{Mo}$  data do hint at a periodic origin. The duration of the  $\delta^{98/95}\text{Mo}$  fluctuations can be evaluated by assigning age constraints to specific points within the stratigraphic record at Site 367. Subsequently, sedimentation rates can be interpolated between these points. Two approaches to assigning age-control points are possible. First, the duration between the onset of the CIE and the Cenomanian–Turonian (C/T) boundary has been estimated to lie between  $\sim 510$  and  $613$  kyr (Sageman et al., 2006; Voigt et al., 2008; Meyers et al., 2012; Ma et al., 2014). Making the assumption that the C/T boundary lies close to the top of core 18 at Site 367 (636.50 mbsf), and placing

the onset of the CIE at 642.16 mbsf from the  $\delta^{13}\text{C}_{\text{org}}$  stratigraphy (point A, Fig. 2), an average sedimentation rate of  $0.9\text{--}1.1$  cm/kyr can be calculated. Applying these sedimentation rates to the three well-defined cycles in  $\delta^{98/95}\text{Mo}$  at the top of the studied section (labelled 1–3, Fig. 2) produces event durations between  $\sim 60$  and  $95$  kyrs. The second approach to assigning age-control points is to transfer radio-isotopically and cyclostratigraphically constrained datum levels to tie-points A and C, which suggests that these points span  $\sim 240\text{--}270$  kyr (Sageman et al., 2006; Ma et al., 2014, Fig. 2). Using these durations gives sedimentation rate estimates of  $0.8\text{--}0.9$  cm/kyr for Site 367, which when applied to the same three cycles in  $\delta^{98/95}\text{Mo}$  discussed above, yields cycle durations between  $\sim 75$  and  $110$  kyr.

Three lines of reasoning suggest that these cycle duration estimates are likely to be too high. Firstly, the estimated sedimentation rates for the three cycles in the 'plateau' interval of Site 367 (Fig. 2) are probably too low. This argument is based on two considerations: (i) The C/T boundary is likely to be located stratigraphically higher than the top of core 18 at Site 367; and (ii) The sedimentation rates extrapolated from the interval between tie-points A and C are not applicable to the 'plateau' of the CIE, due to the  $\sim 5$ -fold increase in organic-carbon abundance after point C (Fig. 2). Underestimating the sedimentation rate for the plateau interval of the CIE would produce cycle durations that were too long. The second line of reasoning is that there are up to nine cycles in  $\delta^{98/95}\text{Mo}$  between tie-point A and the top of core 18. If these cycles were related to eccentricity forcing, as implied by the sedimentation rates calculated above, then the duration of OAE-2 captured at Site 367 would be  $>900$  kyr, which is inconsistent with previous estimates of between  $510$  and  $613$  kyr (Sageman et al., 2006; Voigt et al., 2008;



Meyers et al., 2012; Ma et al., 2014). The third line of reasoning is that previous studies of proto-North Atlantic Ocean sedimentary successions (at DSDP Sites 105 and 603) have found a strong obliquity periodicity in black shale–marlstone deposition (Kuypers et al., 2004; Meyers et al., 2012), that have been related to changes in the chemocline depth, dissolved sulphide concentrations and/or basin residence time. The processes that controlled the sedimentary cycles at Sites 105 and 603 can be hypothetically linked to the  $\delta^{98/95}\text{Mo}$  cycles at Site 367, via the conceptual model outlined in Fig. 4. That these cycles are not clearly expressed in % TOC at Site 367 (Fig. 2) is probably due to the already very high TOC abundances at this location. Instead, the cycles are best expressed in the geochemical parameters (Mo/U and  $\delta^{98/95}\text{Mo}$ ) that are most indicative of dissolved sulphide concentrations and chemocline dynamics.

In summary, cyclic variations in the  $\delta^{98/95}\text{Mo}$  data at Site 367 point to a periodic pacing of the proto-North Atlantic Ocean dissolved Mo inventory and/or in basin dissolved  $\text{H}_2\text{S}$  concentrations. These fluctuations can be linked to observations of sedimentary cycles in the northern proto-North Atlantic that imply a basin-scale response to these processes. Two possibilities for the driving mechanisms behind these periodic fluctuations could be a sea-level control on the exchange of proto-North Atlantic basin seawater with the global ocean, or variable weathering rates of the pan-Atlantic Ocean landmasses that altered the nutrient content (and productivity) of proto-North Atlantic Ocean seawater.

### 4.3. Plenus Cold Event

The interval of low  $\delta^{98/95}\text{Mo}$  between 640.99 and 640.18 mbsf at Site 367 corresponds to a reversal in the CIE, and a drop in sea-surface temperatures recorded by  $\text{TEX}_{86}$  (Forster et al., 2007). These features allow a correlation of the  $\delta^{98/95}\text{Mo}$  excursion to the Plenus Cold Event (Gale and Christensen, 1996; Keller and Pardo, 2004; Tsikos et al., 2004; Jarvis et al., 2006; Friedrich, 2010; Jarvis et al., 2011; Eldrett et al., 2014). This regionally significant event has been linked to surface-water cooling (Forster et al., 2007; van Bentum et al., 2012) associated with a southwards migration of a characteristic macrofauna and watermasses from polar regions (Gale and Christensen, 1996; Zheng et al., 2013) and the re-population of benthic foraminifera at several northern hemisphere locations (Leckie et al., 1998; Kuhnt et al., 2005; Friedrich et al., 2006; Friedrich, 2010; Eldrett et al., 2014) shortly after the initiation of OAE-2. The interval of lower  $\delta^{98/95}\text{Mo}$  during the Plenus Cold Event at Site 367 is not consistent with oxic re-ventilation of the basin deepwater, because the enrichment factor of Mo remains very high (Scott and Lyons, 2012). The relatively lower  $\delta^{98/95}\text{Mo}$  values in this interval do, however, point to a shift in the redox chemistry of the deep proto-North Atlantic Ocean. It can be speculated that the nature of this perturbation involved a decrease in concentrations of dissolved  $\text{H}_2\text{S}$ , which altered the distribution of thiomolybdate species (and thus isotopic composition of Mo) being deposited. A decrease in  $\text{H}_2\text{S}$

concentrations might also point to a transient deepening of the chemocline.

The most prominent feature of the Tarfaya  $\delta^{98/95}\text{Mo}$  record is a 0.90‰ excursion to lower values. The excursion corresponds to a reduction in millimetre-scale sedimentary lamination, and an increase in the quantity of benthic foraminifera in the deepest parts of the basin (Kuhnt et al., 2005). The observation that the excursion took place shortly following the last occurrence of the planktonic foraminifera *Rotalipora cushmani*, and after the first positive peak in the CIE (Kuhnt et al., 2005), allows the  $\delta^{98/95}\text{Mo}$  excursion to also be correlated with the Plenus Cold Event. The  $\delta^{98/95}\text{Mo}$  values and Mo enrichment factors at S57 are much lower than for this interval at Site 367. The very low  $\delta^{98/95}\text{Mo}$  suggest that Mo was removed from the basin by adsorption to Fe- and Mn-oxyhydroxides, which fractionate Mo by -0.80–3.00‰ from seawater (Siebert et al., 2003; Barling and Anbar, 2004; Wasylenki et al., 2008; Goldberg et al., 2009). The apparent stability of such oxyhydroxide minerals in the Tarfaya basin during the Plenus Cold Event points to a significant basin seawater ventilation episode that re-oxygenated deeper waters. In summary, the Plenus Cold Event appears to have affected the redox chemistry of both the Tarfaya Basin and the deep proto-North Atlantic Ocean, but the size of this perturbation towards more oxygenated conditions was more pronounced in the shallower (and less hydrographically ‘buffered’) Tarfaya Basin.

### 4.4. Mo-isotope constraints on global redox

Sediments at Site 367 were deposited underneath a quasi-stable euxinic watermass (Sinninghe Damsté and Koster, 1998; Kuypers et al., 2002; Pancost et al., 2004), in a large hydrographically restricted basin (Jenkyns, 2010; Trabucho Alexandre et al., 2010; Westermann et al., 2014), with evidence for a control of sedimentary  $\delta^{98/95}\text{Mo}$  compositions by the dissolved basin seawater Mo inventory, the concentration of dissolved  $\text{H}_2\text{S}$ , and/or the basin seawater residence time in the southern proto-North Atlantic Ocean (Figs. 4 and 5). These observations strongly suggest that the maximum measured sedimentary  $\delta^{98/95}\text{Mo}$  isotope composition of 1.20‰ approximates the time-equivalent global seawater  $\delta^{98/95}\text{Mo}$  for OAE-2. A second constraint on the global seawater Mo-isotope composition during OAE-2 is the observation that the  $\delta^{98/95}\text{Mo}$  of anoxic sediments deposited under more Mo-replete conditions in the Tarfaya Basin were ~0.7‰ lower than the time-equivalent composition inferred from the Site 367 data, in line with the expected fractionation between seawater Mo and Mo-sulphides (Poulson-Brucker et al., 2009, 2012). It is unlikely that the highest Mo-isotope composition at Site 367 simply records the average riverine flux to the proto-North Atlantic Ocean, because the large difference in the Mo concentrations of seawater and river waters at the present day (105  $\mu\text{mol/l}$  versus ~5  $\mu\text{mol/l}$  respectively (Siebert et al., 2003; Archer and Vance, 2008)) would require an almost complete severing of any seawater connection with the global ocean for the riverine flux to dominate. Even if the global seawater Mo concentration were

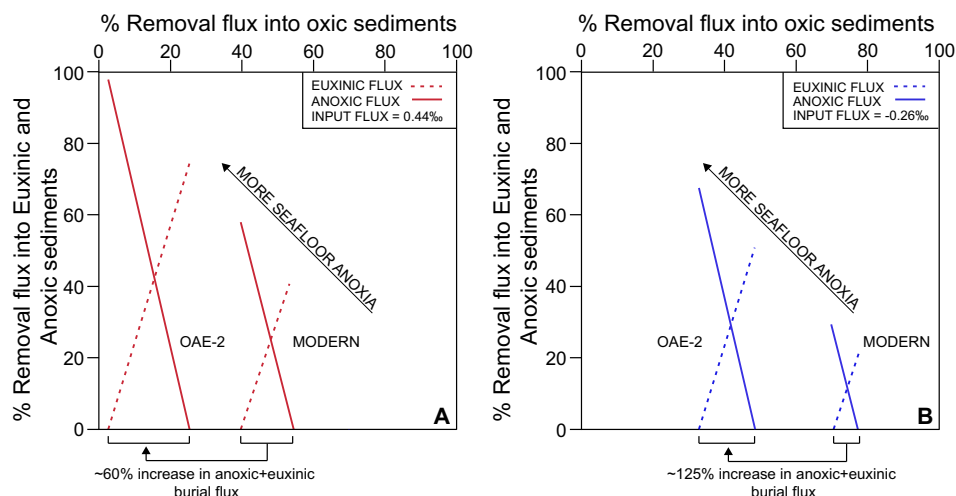


Fig. 6. Estimates of the Mo removal fluxes into different seafloor redox environments assuming: (A) a weighted average global riverine Mo flux of  $0.44\text{‰}$  (Archer and Vance, 2008), and (B) a weighted average global riverine Mo flux of  $-0.26\text{‰}$ , equal to mafic rocks (Siebert et al., 2003). Lines indicate the proportion of the global seawater Mo-removal flux going into euxinic, anoxic and oxic seafloor sediments. A change towards a greater global removal flux of Mo into anoxic or euxinic seafloor environments would shift the lines towards the top and left of each plot. The arrows below each plot show the average increase, relative to present, in the flux of Mo into anoxic and euxinic seafloor sediments required to achieve a Mo cycle in steady state for a seawater composition of  $1.2\text{‰}$  during OAE-2. The plots highlight the relatively wide spread in Mo removal fluxes that could achieve the same seawater Mo-isotope composition, but nonetheless confirm a shift to overall more reducing conditions at a global scale.

10-fold lower than at present, Mo delivered by exchange over marginal seaways would still dominate the input flux of Mo to the proto-North Atlantic Basin.

The new Mo-isotope data can be used to estimate the magnitude of the different Mo removal fluxes, assuming a steady-state balance between Mo-input fluxes (Archer and Vance, 2008; Pearce et al., 2010; Neubert et al., 2011) and the different redox-dependent removal pathways into seafloor sediments. The Mo flux into oxygenated sediments may be approximated by assuming that the dominant process was the adsorption of  $\text{MoO}_4^{2-}$  to Mn-oxyhydroxides, which fractionates Mo by  $\sim -3\text{‰}$  from its seawater value (Siebert et al., 2003; Barling and Anbar, 2004). Adsorption to Fe-oxyhydroxides (Goldberg et al., 2009) may also have been important, but the relative importance of Fe- versus Mn-oxyhydroxides at a global scale during OAE-2 is difficult to quantify. The use of three redox-dependent removal pathways for Mo rather than two (e.g. Ling et al., 2005; Pearce et al., 2008) creates multiple combinations of euxinic and anoxic Mo-fluxes that can create the same seawater  $\delta^{98/95}\text{Mo}$ . The range of these fluxes can be modelled by assuming a steady-state balance between the input fluxes of Mo to the ocean, and the three redox-dependent output fluxes to marine sediments (c.f. Poulson-Brucker et al., 2009; Dickson et al., 2014). A range of removal fluxes can then satisfy the isotopic constraints on the global mass balance of Mo (Fig. 6). The mass-balance equations for steady-state Mo concentrations and isotope ratios with constant fluxes in oxic, anoxic, and euxinic regions are:

$$\begin{aligned} & (^{98}\text{Mo}/^{95}\text{Mo})_{\text{sw}} \times (\alpha_{\text{ox}}f_{\text{ox}} + \alpha_{\text{anox}}f_{\text{anox}} + \alpha_{\text{eux}}f_{\text{eux}}) \\ &= (^{98}\text{Mo}/^{95}\text{Mo})_{\text{In}} \end{aligned} \quad (1)$$

and

$$f_{\text{ox}} + f_{\text{anox}} + f_{\text{eux}} = 1 \quad (2)$$

where the ratios  $(^{98}\text{Mo}/^{95}\text{Mo})_{\text{sw}}$  and  $(^{98}\text{Mo}/^{95}\text{Mo})_{\text{In}}$  are the isotopic ratios of global seawater and of Mo input fluxes, the latter mainly from rivers (Archer and Vance, 2008).  $f_{\text{ox}}$ ,  $f_{\text{anox}}$ , and  $f_{\text{eux}}$  are the fractions of the total Mo flux to sediments under oxic, anoxic, and euxinic conditions, respectively. The fractionation factors between sedimenting particles and seawater are  $\alpha_{\text{ox}} = (^{98}\text{Mo}/^{95}\text{Mo})_{\text{sed}} / (^{98}\text{Mo}/^{95}\text{Mo})_{\text{sw}}$ , and similarly for anoxic and euxinic environments. A range of Mo removal fluxes ( $f_{\text{ox}}$ ,  $f_{\text{anox}}$ ,  $f_{\text{eux}}$ ) can be found to balance Eq. (1) (solid and dashed lines in Fig. 6) for different assumptions of  $(^{98}\text{Mo}/^{95}\text{Mo})_{\text{In}}$  (Fig. 6a and b), showing that there is not a unique solution to the extent of Mo removal into low-oxygen settings for a given seawater composition. However, even if the quantitative removal estimates have a high uncertainty, the results do clearly demonstrate a shift towards more extensive Mo removal into anoxic and euxinic sediments, which on average was  $\sim 60\text{--}125\%$  higher than at the present day.

A final consideration based on Fig. 2 is that if the highest  $\delta^{98/95}\text{Mo}$  values of  $\sim 1.20\text{‰}$  reached during the plateau interval of OAE-2 at Site 367 do approximate the global seawater composition, then the first instance of this value occurs extremely close to the onset of the CIE – just two data points after point ‘A’ (Fig. 3). The early timing of this

Table 1  
Raw data for DSDP site 367.

Core	Section	Top_depth	Bottom_depth	Metres composite depth (corr)	$\delta^{13}\text{C}_{\text{org}}$	TOCnorm	Mo (ppm)	U (ppm)	Al (ppm)	$\delta^{98/95}\text{Mo}$	2 SE
<i>DSDP site 367</i>											
18	1	50	51	636.50	−22.30	33.40	97.41	23.00	73,082	0.64	0.04
18	1	56	57	636.56	−23.53	43.23	375.82	20.98	48,500		
18	1	63	64	636.63	−20.31	33.74	150.95	34.05	22,314	0.67	0.03
18	1	70	71	636.70	−21.29	35.63	90.96	29.47	28,036	1.09	0.03
18	1	78	79	636.78	−21.48	24.84	79.88	36.48	46,313	0.96	0.04
18	1	86	87	636.86	−22.50	47.02	111.93	21.04	14,690	0.82	0.02
18	1	94	95	636.94	−21.47	48.36	96.27	18.90	18,780		
18	1	101	102	637.01	−22.45	34.98	104.51	16.79	33,169	0.55	0.04
18	1	108	109	637.08	−21.91	30.20	132.31	21.56	27,423	0.43	0.03
18	1	118	119	637.18	−21.44	47.25	75.72	30.77	14,530		
18	1	126	127	637.26	−22.85	43.66	143.81	29.03	18,526	0.72	0.03
18	1	133	134	637.33	−23.27	41.01	168.18	19.60	28,206	0.46	0.03
18	1	140	141	637.40	−21.79	33.09	100.53	19.07	19,807		
18	1	146	147	637.46	−23.14	43.30	124.66	19.46	17,729	0.65	0.02
18	2	2	3	637.52	−22.42	43.59	73.00	16.51	16,309	1.21	0.02
18	2	10	11	637.60	−22.20	31.12	63.17	19.74	29,206	1.09	0.03
18	2	18	20	637.68	−24.74	35.23	95.58	24.96	17,915		
18	2	26	27	637.76		19.59	59.96	22.27	34,888	1.01	0.02
18	2	33	34	637.83	−21.70	40.73	77.22	29.14	22,977		
18	2	39	40	637.89	−22.08	22.70	275.01	20.64	35,658	0.82	0.04
18	2	46	47	637.96		7.21	35.12	10.14	50,049	0.69	0.07
18	2	54	55	638.04	−22.33	34.18	338.92	37.44	15,894	0.49	0.06
18	2	61	62	638.11	−21.43	44.79	280.76	29.24	18,307		
18	2	68	69	638.18	−22.72	33.56	159.99	20.42	32,340	0.63	0.02
18	2	76	77	638.26	−23.65	38.78	139.76	25.76	26,940		
18	2	85	86	638.35	−22.00	24.98	108.07	41.38	20,827	0.91	0.07
18	2	90	91	638.40	−21.93	38.16	103.99	23.62	23,214	0.98	0.04
18	2	96	97	638.46	−21.94	35.83	117.66	24.44	21,322	0.97	0.03
18	2	103	104	638.53	−21.98	37.90	103.45	29.20	21,911	0.94	0.07
18	2	110	111	638.60	−21.77	34.35	189.09	19.15	16,357	0.74	0.06
18	2	118	119	638.68	−21.78	46.57	135.20	27.35	16,327		
18	2	124	125	638.74	−22.99	22.94	109.36	12.92	30,159	0.52	0.03
18	2	131	132	638.81	−21.86	19.37	54.99	15.80	37,857	0.50	0.03
18	2	141	142	638.91	−21.75	26.61	53.71	20.46	20,501		
18	2	148	149	638.98	−21.89	27.90	50.55	28.24	29,986	1.04	0.05
18	2	156	157	639.06	−22.01	42.66	75.26	41.43	15,275	1.06	0.03
18	2	162	163	639.12	−22.09	28.68	63.87	30.22	32,134	0.90	0.03
18	3	1	2	639.14	−22.42	25.70	97.88	17.35	28,180	0.84	0.05
18	3	9	10	639.22	−22.31	27.24	94.78	16.77	29,047	0.87	0.06
18	3	17	18	639.30	−22.57	24.80	101.45	16.01	29,559		
18	3	23	24	639.36	−20.66	32.26	182.24	23.51	28,074	0.89	0.04
18	3	30	31	639.43	−22.08	31.30	189.40	11.77	23,235	0.52	0.03
18	3	39	40	639.52	−21.78	31.78	56.72	7.57	34,570		
18	3	46	47	639.59	−22.21	28.59	54.55	28.20	24,791	0.87	0.04
18	3	53	54	639.66	−22.14	30.05	50.60	21.47	31,390	0.88	0.06
18	3	61	62	639.74	−22.01	39.96	116.71	17.47	18,484	0.96	0.08
18	3	68	69	639.81	−22.11	31.78	137.20	21.01	33,763	0.25	0.04
18	3	73	74	639.86	−21.96	28.48	89.43	3.44	28,682	0.74	0.03
18	3	84	85	639.97	−22.50	42.27	27.20	36.70	22,908		
18	3	90	91	640.03	−21.61	41.83	18.53	20.10	19,526	0.95	0.03
18	3	98	99	640.11	−22.79	40.37	63.01	19.44	19,678	1.08	0.06
18	3	105	106	640.18	−23.91	29.24	93.44	12.73	24,097	0.47	0.03
18	3	112	113	640.25	−25.22	11.73	50.40	14.98	52,541		
18	3	118	119	640.31	−21.95	53.34	81.96	39.58	11,828	0.28	0.03
18	3	126	127	640.39	−22.73	45.99	78.60	37.24	22,581	0.48	0.08
18	3	134	135	640.47	−22.47	52.05	108.52	28.02	16,613		
18	3	140	141	640.53	−23.49	55.98	96.50	32.25	17,455	0.21	0.03
18	3	147	148	640.60	−22.64	54.60	78.02	34.99	15,222	0.52	0.08
18	4	6	7	640.69	−25.00	25.18	249.78	25.97	35,295		

(continued on next page)

Table 1 (*continued*)

Core	Section	Top_depth	Bottom_depth	Metres composite depth (corr)	$\delta^{13}\text{C}_{\text{org}}$	TOCnorm	Mo (ppm)	U (ppm)	Al (ppm)	$\delta^{98/95}\text{Mo}$	2 SE
18	4	12	13	640.75	−24.97	35.15	473.40	41.48	29,494	0.27	0.06
18	4	19	20	640.82	−25.54	33.82	232.66	21.72	30,027	0.47	0.05
18	4	27	28	640.90	−26.55	43.18	276.78	0.01	22,279		
18	4	36	37	640.99	−24.74	36.40	162.53	38.98	24,416	0.87	0.03
18	4	43	44	641.06	−24.25	39.95	165.13	53.22	21,292	1.00	0.04
18	4	51	52	641.14	−23.05	52.49	631.74	124.60	11,105		
18	4	59	60	641.22	−26.75	15.81	69.13	10.49	50,557	0.40	0.03
18	4	68	69	641.31	−25.46	46.43	132.21	48.18	19,568	0.97	0.05
18	4	75	76	641.38	−22.22	47.99	294.49	101.99	14,697		
18	4	86	87	641.49	−25.22	40.15	115.64	29.40	28,905	0.85	0.03
18	4	94	95	641.57	−25.08	21.77	107.70	36.48	30,889	1.06	0.03
18	4	104	105	641.67	−24.04	34.77	172.89	34.79	20,761		
18	4	113	114	641.76	−26.21	23.07	141.45	30.09	33,949	0.61	0.02
18	4	124	125	641.87	−25.62	25.27	165.99	27.43	37,283		
18	4	134	135	641.97	−25.98	19.27	137.65	20.59	35,210	1.17	0.02
18	4	142	143	642.05	−25.34	16.78	270.69	27.07	53,214	0.91	0.03
18	4	153	154	642.16	−28.01	5.64	40.00	4.59	49,068	0.36	0.03
18	5	11	12	642.24	−28.03	5.08	32.65	8.84	62,860		
18	5	21	22	642.34	−27.96	6.31	24.16	4.76	55,130	0.34	0.02
18	5	31	32	642.44	−27.91	4.27	19.55	5.61	63,478	0.36	0.02
18	5	39	40	642.52	−27.92	4.32	21.38	4.74	60,165		
18	5	46	47	642.59	−27.70	7.05	33.51	6.10	66,002	0.33	0.04
18	5	55	56	642.68	−28.19	13.54	99.82	14.05	50,125	0.08	0.02
18	5	63	64	642.76	−27.88	30.98	62.87	10.24	70,428		
18	5	72	73	642.85	−28.37	6.37	80.42	11.53	37,595	−0.07	0.03
18	5	82	83	642.95	−28.38	14.29	91.14	11.30	33,695	−0.07	0.03
18	5	87	88	643.00	−28.10	2.63	25.67	2.70	67,721		
18	5	97	98	643.10	−28.29	27.24	238.97	26.34	49,228	0.06	0.04
18	5	106	107	643.19	−28.19	14.23	95.90	12.14	44,608		
18	5	118	119	643.31	−27.59	19.30	329.55	38.73	95,667	0.38	0.06
18	5	127	128	643.40	−27.27	2.97	21.91	4.18	62,026	0.30	0.04
18	5	136	137	643.49	−26.69	1.11	19.37	3.35	68,761	0.37	0.03
18	5	148	149	643.61	−27.15	6.54	40.90	6.49	64,726		
19	1	137	138	646.00	−27.47	3.96	39.51	7.57	73,232	0.18	0.04
19	1	147	148	646.10	−27.76	13.95	144.05	10.71	54,685		
19	2	8	9	646.21	−26.50	31.38	321.40	41.80	32,716	0.12	0.06
19	2	16	17	646.29	−27.53	12.25	187.41	14.29	49,790		
19	2	25	26	646.38	−28.33	16.92	206.76	22.53	45,847		
19	2	35	36	646.48	−28.29	18.81	200.92	17.36	30,081	0.03	0.04
19	2	44	45	646.57	−28.41	5.42	45.83	4.26	76,123		
19	2	54	55	646.67	−27.94	5.90	24.86	4.29	61,388	0.33	0.06
19	2	63	64	646.76	−28.06	5.09	16.90	4.64	71,849		
19	2	73	74	646.86	−28.25	10.20	93.15	10.77	56,884	−0.03	0.06
19	2	73	74	646.86						−0.03	0.04
19	2	83	84	646.96	−28.22	7.62	72.17	6.80	72,528		
19	2	93	94	647.06	−27.91	2.25	18.77	4.44	64,526		
19	2	104	105	647.17	−27.72	7.71	66.00	8.83	75,944	0.08	0.04
19	2	113	114	647.26	−27.81	5.03	38.53	8.00	65,278		
19	2	123	124	647.36	−27.84	9.62	84.60	16.02	66,912		
19	2	133	134	647.46	−27.35	7.53	34.23	7.63	53,331	0.11	0.06
19	2	142	143	647.55	−27.55	1.66	18.48	5.71	70,521		
19	2	150	151	647.63	−28.07	2.65	19.05	6.54	64,604		
19	3	10	11	647.73	−28.07	5.71	58.29	10.58	76,207	0.19	0.03
19	3	20	21	647.83	−27.92	18.89	113.32	20.89	43,394		
19	3	30	31	647.93	−28.25	8.69					

Metres composite depth scale has been calculated to correct for core expansion during storage.

first maximum value suggests that the expansion of seafloor redox must have happened extremely quickly at the start of the event, or that expansion of seafloor anoxia and euxinia

began prior to the CIE. The latter suggestion is consistent with increases in trace-metal enrichments occurring in Cenomanian black shales underlying the CIE at Demerara

Table 2  
Raw data for Tarfaya Basin core S57.

Depth (m)	$\delta^{98/95}\text{Mo}$	2 SE uncertainty	Mo (ppm)
<i>Tarfaya core S57</i>			
30.04	0.58	0.03	18.02
31.67	0.40	0.03	18.62
35.03	0.98	0.03	20.00
37.52	0.72	0.03	17.12
40.07	0.37	0.03	8.62
41.22	0.59	0.03	7.44
44.81	0.44	0.05	6.87
45.74	0.46	0.06	2.22
47.84	0.41	0.03	30.09
49.13	0.69	0.06	30.17
49.96	0.50	0.07	46.52
50.96	0.56	0.02	2.47
51.13	0.91	0.06	3.84
51.55	−0.39	0.04	1.64
51.92	0.64	0.06	5.34
52.30	−0.07	0.02	3.36
52.70	0.07	0.08	1.03
52.92	0.35	0.03	1.14
53.52	0.51	0.05	0.75
53.96	0.44	0.03	31.48
54.53	0.39	0.07	3.44
55.34	0.52	0.07	2.32
55.90	0.70	0.07	19.10
56.72	0.28	0.06	3.25
58.16	0.73	0.04	19.60
59.35	0.77	0.04	63.38

Rise (Hetzel et al., 2009). The magnitude by which seafloor anoxia expanded compared to the pre-OAE extent requires future estimates of the late Cenomanian Mo-isotope composition of global seawater (See Table 1).

## 5. CONCLUSIONS

New Mo-isotope records from two sites spanning Late Cretaceous OAE-2 are presented. The highly resolved record from DSDP Site 367 demonstrates periodic changes in the sediment  $\delta^{98/95}\text{Mo}$ , with an amplitude of  $\sim 0.65\%$ . These cycles can be hypothetically linked to basin-scale changes in dissolved sulphide concentrations, the dissolved inventory of Mo, and the chemocline depth in the proto-North Atlantic Ocean. It is likely that these oscillations have a periodic component related to orbital obliquity. Correlation of the  $\delta^{98/95}\text{Mo}$  cycles at Site 367 to sedimentary cycles at DSDP Sites 105 and 603 suggest that obliquity-driven oscillations in redox and productivity were a basin-wide feature of the proto-North Atlantic Ocean during OAE-2. These features may have been associated with changes in sea level and/or changes in chemical weathering intensity that would have controlled the flux of dissolved Mo into the basin, and would have provided a source of nutrients to stimulate primary productivity.

The  $\delta^{98/95}\text{Mo}$  data also have value as a stratigraphic marker for the Plenius Cold Event in the Tarfaya and Cape Verde Basins during the early phase of OAE-2, and thus link redox changes at these locations to a period not only

of probable global cooling but also inferred northern hemisphere volcanic activity (e.g. Zheng et al., 2013; Eldrett et al., 2014).

The new  $\delta^{98/95}\text{Mo}$  data allow the global removal fluxes of Mo into anoxic and euxinic seafloor sediments to be calculated for OAE-2. Mo removal fluxes into sediments with sulphidic pore-waters (including those overlain by euxinic and non-euxinic seawater) were approximately 60–125% higher than at the present day, which would translate to <10% of the global seafloor area (c.f. Ling et al., 2005; Archer and Vance, 2008). These figures are less than the >35-fold increase in seafloor euxinia estimated from sulphur-isotope modelling of sulphate reduction and pyrite fixation during OAE-2 (Owens et al., 2013), but similar to a recent estimate based on low-resolution Mo-isotope measurements of the more oxidized working half of Site 367 (Westermann et al., 2014). These estimates demonstrate that, although OAE-2 was a significant global carbon-burial event characterized by a large expansion of seafloor anoxia and euxinia, large areas of the global seafloor probably remained largely untouched by the spread of deoxygenated watermasses. The stratigraphic record is informative: although Cenomanian–Turonian organic-rich shales are recorded from paleo-Equatorial Pacific drilling sites (Schlanger et al., 1987), certain environments around the Pacific Rim were dominantly oxic during the OAE, as also were parts of Europe (Wiese, 2009; Westermann et al., 2010; Takashima et al., 2011; Hasegawa et al., 2013).



## ACKNOWLEDGEMENTS

We thank Alan Hsieh and Mabs Gilmour for laboratory support, Cinzia Bottini for help in sampling the Site 367 core, Sadat Kolonic for providing raw data, James Eldrett and Gideon Henderson for commenting on early versions of the manuscript, Christopher Pearce and Harilaos Tsikos for providing constructive reviews and Shell for research funding. Samples from Site 367 were provided by the International Ocean Discovery Program.

## REFERENCES

- Adams D. D., Hurtgen M. T. and Sageman B. B. (2010) Volcanic triggering of a biogeochemical cascade during Oceanic Anoxic Event 2. *Nat. Geosci.* **3**, 201–204.
- Algeo T. J. and Lyons T. W. (2006) Mo–total organic carbon covariation in modern anoxic marine environments: implications for analysis of paleoredox and paleohydrologic conditions. *Paleoceanography* **21**, PA1016. <http://dx.doi.org/10.1029/PA001112>.
- Algeo T. J. and Tribouillard N. (2009) Environmental analysis of paleoceanographic systems based on molybdenum–uranium covariation. *Chem. Geol.* **268**, 211–225.
- Archer C. and Vance D. (2008) The isotopic signature of the global riverine molybdenum flux and anoxia in the ancient oceans. *Nat. Geosci.* **1**, 597–600.
- Arthur M. A., Jenkyns H. C., Brumsack H. and Schlanger S. O. (1990) Stratigraphy, geochemistry, and paleoceanography of organic-carbon-rich Cretaceous sequences. In *Cretaceous Resources, Events and Rhythms*, vol. 304 (eds. R. N. Ginsburg and B. Beaudoin), pp. 75–119. NATO ASI Series. Kluwer Academic Publishers, Dordrecht.
- Barling J. and Anbar A. D. (2004) Molybdenum isotope fractionation during adsorption by manganese oxides. *Earth Planet. Sci. Lett.* **217**, 315–329.
- Blättler C. L., Jenkyns H. C., Reynard L. M. and Henderson G. M. (2011) Significant increases in global weathering during Oceanic Anoxic Events 1a and 2 indicated by calcium isotopes. *Earth Planet. Sci. Lett.* **309**, 77–88.
- Čepek P. (1978) Mesozoic calcareous nannoplankton of the eastern North Atlantic, Leg 41. In *Initial Reports of the Deep Sea Drilling Project* (eds. Y. Lancelot, E. Seibold, et al.), vol. 41, pp. 667–687. US Government Printing Office, Washington.
- Chappaz A. et al. (2014) Does pyrite act as an important host for molybdenum in modern and ancient euxinic sediments? *Geochim. Cosmochim. Acta* **126**, 112–122.
- Crusius J., Calvert S., Pedersen T. and Sage D. (1996) Rhenium and molybdenum enrichments in sediments as indicators of oxic, suboxic and sulphidic conditions of deposition. *Earth Planet. Sci. Lett.* **145**, 65–78.
- Dahl T., Anbar A. D., Gordon G. W., Rosing M. T., Frei R. and Canfield D. E. (2010) The behaviour of molybdenum and its isotopes across the chemocline and in the sediments of sulphidic Lake Cadagno, Switzerland. *Geochim. Cosmochim. Acta* **74**, 144–163.
- Dickson A. J., Cohen A. S. and Coe A. L. (2014) Continental margin molybdenum isotope signatures from the early Eocene. *Earth. Planet. Sci. Lett.* **405**.
- Du Vivier A. D. C. et al. (2014) Marine  $^{187}\text{Os}/^{188}\text{Os}$  isotope stratigraphy reveals the interaction of volcanism and ocean circulation during Oceanic Anoxic Event 2. *Earth Planet. Sci. Lett.* **389**, 23–33.
- Eldrett J. S., Minisini D. and Bergman S. C. (2014) Decoupling of the carbon cycle during Oceanic Anoxic Event 2. *Geology* **42**, 567–570.
- Eldrett J. S., Ma C., Bergman S. C., Lutz B., Gregory F. J., Dodsworth P., Phipps M., Hardas P., Minisini D., Ozkan A., Ramezani J., Bowring S. A., Kamo S. L., Ferguson K., Macaulay C. and Kelly A. (2015) An astronomically calibrated stratigraphy of the Cenomanian, Turonian and earliest Coniacian from the Cretaceous Western Interior Seaway, USA: implications for global astrochronology. *Cretaceous Res.* **56**, 316–344.
- Emerson S. R. and Huested S. S. (1991) Ocean anoxia and the concentrations of molybdenum and vanadium in seawater. *Mar. Chem.* **34**, 177–196.
- Eriksson B. E. and Helz G. R. (2000) Molybdenum (IV) speciation in sulphidic waters: stability and lability of thiomolybdates. *Geochim. Cosmochim. Acta* **64**, 1149–1158.
- Forster A., Schouten S., Moriya K., Wilson P. A. and Sinninghe Damsté J. S. (2007) Tropical warming and intermittent cooling during the Cenomanian/Turonian oceanic anoxic event 2: Sea surface temperature records from the equatorial Atlantic. *Paleoceanography* **22**, PA1219. <http://dx.doi.org/10.1029/PA001349>.
- Friedrich O. (2010) Benthic foraminifera and their role to decipher paleoenvironment during mid-Cretaceous Oceanic Anoxic Events – the “anoxic benthic foraminifera” paradox. *Rev. Micropaléontol.* **53**, 175–192.
- Friedrich O., Erbacher J. and Mutterlose J. (2006) Paleoenvironmental change across the Cenomanian/Turonian Boundary Event [Oceanic Anoxic Event 2] as indicated by benthic foraminifera from the Demerara Rise [ODP Leg 207]. *Rev. Micropaléontol.* **49**, 121–139.
- Frijia G. and Parente M. (2008) Strontium isotope stratigraphy in the upper Cenomanian shallow-water carbonates of the southern Apennines: Short-term perturbations of marine  $^{87}\text{Sr}/^{86}\text{Sr}$  during the oceanic anoxic event 2. *Palaeogeogr., Palaeoclimatol., Palaeoecol.* **261**, 15–29.
- Gale A. S. and Christensen W. K. (1996) Occurrence of the belemnite *Actinocamax plenus* in the Cenomanian of SE France and its significance. *Bull. Geol. Soc. Den.* **43**, 68–77.
- Goldberg T., Archer C., Vance D. and Poulton S. W. (2009) Mo isotope fractionation during adsorption to Fe (oxyhydr)oxides. *Geochim. Cosmochim. Acta* **73**, 6502–6516.
- Goldberg T., Archer C., Vance D., Thamdrup B., McAnena A. and Pultson S. W. (2012) Controls on Mo isotope fractionations in a Mn-rich anoxic marine sediment, Gullmar Fjord, Sweden. *Chem. Geol.* **296**, 73–86.
- Goldberg T. et al. (2013) Resolution of inter-laboratory discrepancies in Mo isotope data: an intercalibration. *J. Anal. At. Spectrom.* **28**, 724–735.
- Greber N. D., Siebert C., Nögler T. F. and Petke T. (2012) 98/95Mo values and Molybdenum concentration data for NIST SRM 610, 612 and 3134: towards a common protocol for reporting Mo data. *Geostand. Geoanal. Res.* **36**, 291–300.
- Hasegawa T. (1997) Cenomanian–Turonian carbon isotope events recorded in terrestrial organic matter from northern Japan. *Palaeogeogr., Palaeoclimatol., Palaeoecol.* **130**, 251–273.
- Hasegawa T. et al. (2013) Carbon isotope stratigraphy and depositional oxia through Cenomanian–Turonian boundary sequences (Upper Cretaceous) in New Zealand. *Cretaceous Res.* **40**, 61–80.
- Helz G. R., Bura-Nakić E., Mikac N. and Ciglenečki I. (2011) New model for molybdenum behavior in euxinic waters. *Chem. Geol.* **284**, 323–332.
- Herbin J.-P., Masure E. and Roucaché J. (1987) Cretaceous formations from the lower continental rise off Cape Hatteras: Organic geochemistry, dinoflagellate cysts, and the Cenomanian/Turonian boundary event at Sites 603 (Leg 93) and 105 (Leg 11). In *Initial Reports of the Deep Sea Drilling Project*.

- (eds. J.E. van Hinte, S.W. Jr. Wise, et al.), vol. 93, pp. 1139–1162. Washington (U.S. Govt. Printing Office). <http://dx.doi.org/10.2973/dsdp.proc.93.147.1987>.
- Hetzel A., Böttcher M. E., Wortmann U. G. and Brumsack H.-J. (2009) Paleo-redox conditions during OAE 2 reflected in Demerara Rise sediment geochemistry (ODP Leg 207). *Palaeogeogr., Palaeoclimatol., Palaeoecol.* **273**, 302–328.
- Jarvis I., Gale A. S., Jenkyns H. C. and Pearce M. A. (2006) Secular variation in late Cretaceous carbon isotopes: a new  $\delta^{13}\text{C}$  carbonate reference curve for the Cenomanian-Campanian (99.6–70.6 Ma). *Geol. Mag.* **143**, 561–608.
- Jarvis I., Lignum J. S., Gröcke D. R., Jenkyns H. C. and Pearce M. A. (2011) Black shale deposition, atmospheric  $\text{CO}_2$  drawdown, and cooling during the Cenomanian-Turonian Oceanic Anoxic Event. *Paleoceanography* **20**, PA3201. <http://dx.doi.org/10.1029/2010PA002081>.
- Jenkyns H. C. (1980) Cretaceous anoxic events: from continents to oceans. *J. Geol. Soc. London* **137**, 171–188.
- Jenkyns H. C. (2003) Evidence for rapid climate change in the Mesozoic-Palaeogene greenhouse world. *Philos. Trans. R. Soc. London A* **361**, 1885–1916.
- Jenkyns H. C. (2010) Geochemistry of oceanic anoxic events. *Geochem. Geophys. Geosyst.* **11**, Q03004. <http://dx.doi.org/10.1029/2009GC002788>.
- Keller G. and Pardo A. (2004) Age and paleoenvironment of the Cenomanian-Turonian global stratotype section and point at Pueblo, Colorado. *Mar. Micropaleontol.* **51**(1–2), 95–128.
- Kolonis S. et al. (2005) Black shale deposition on the northwest African shelf during the Cenomanian/Turonian oceanic anoxic event: Climate coupling and global organic carbon burial. *Paleoceanography* **20**, PA1006. <http://dx.doi.org/10.1029/PA000950>.
- Kuhnt W., Luderer F., Nederbragt S., Thurow J. and Wagner T. (2005) Orbital-scale record of the late Cenomanian-Turonian oceanic anoxic event (OAE-2) in the Tarfaya Basin (Morocco). *Int. J. Earth Sci.* **94**, 147–159.
- Kuhnt W., Nederbragt A. and Leine L. (1997) Cyclicity of Cenomanian-Turonian organic-carbon-rich sediments in the Tarfaya Atlantic Coastal Basin (Morocco). *Cretaceous Res.* **18**, 587–601.
- Kuroda J. et al. (2007) Contemporaneous massive subaerial volcanism and late cretaceous Oceanic Anoxic Event 2. *Earth Planet. Sci. Lett.* **256**, 211–223.
- Kuypers M. M. M., Pancost R. D. and Sinninghe Damsté J. S. (1999) A large and abrupt fall in atmospheric  $\text{CO}_2$  concentration during Cretaceous times. *Nature* **399**, 342–345.
- Kuypers M. M. M., Pancost R. D., Nijenhuis I. A. and Sinninghe Damsté J. S. (2002) Enhanced productivity led to increased organic carbon burial in the euxinic North Atlantic basin during the late Cenomanian oceanic anoxic event. *Paleoceanography* **17**, 1051. <http://dx.doi.org/10.1029/2000PA000569>.
- Kuypers M. M. M. et al. (2004) Orbital forcing of organic carbon burial in the proto-North Atlantic during oceanic anoxic event 2. *Earth Planet. Sci. Lett.* **228**, 465–482.
- Lancelot, Y. (1977) The evolution of the central Northeastern Atlantic – summary of results of DSDP Leg 41. In *Initial Reports of the DSDP* (eds. Lancelot, Y., Seibold, E. and Gardner, J.V.). vol. 41, pp. 1215–1245. Washington (U.S. Government Printing Office).
- Leckie, R.M., Yuretic, R.F., West, O.L.O., Finkelstein, D. and Schmidt, M. (1998) Paleocyanography of the southwestern Western Interior Sea during the time of the Cenomanian-Turonian boundary (late Cretaceous). In *Stratigraphy and Paleoenvironments of the Cretaceous Western Interior Seaway, USA* (eds. Dean, W.A. and Arthur, M.A.). SEPM Concepts in Sedimentology and Paleontology, vol. 6, pp. 101–126.
- Ling H.-F., Gao J.-F., Zhao K.-D., Jiang S.-Y. and Ma D.-S. (2005) Comment on “Molybdenum isotope evidence for widespread anoxia in Mid-Proterozoic oceans”. *Science* **309**, 1017.
- Ma C., Meyers S. R., Sageman B. B., Singer B. S. and Jicha B. R. (2014) Testing the astronomical time scale for oceanic anoxic event 2, and its extension into Cenomanian strata of the Western Interior Basin (USA). *Geol. Soc. Am. Bull.* **126**, 974–989.
- MacLeod K. G., Huber B. T., Jiménez Berrocoso Á. and Wendler I. (2013) A stable and hot Turonian without glacial  $\delta^{18}\text{O}$  excursions is indicated by exquisitely preserved Tanzanian foraminifera. *Geology* **41**, 1083–1086.
- Meyers S. R., Sageman B. B. and Arthur M. A. (2012) Obliquity forcing of organic matter accumulation during Oceanic Anoxic Event 2. *Paleoceanography* **27**, PA3212. <http://dx.doi.org/10.1029/2012PA002286>.
- Miller C. A., Peucker-Ehrenbrink B., Walker B. D. and Marcantonio F. (2011) Re-assessing the surface cycling of molybdenum and rhenium. *Geochim. Cosmochim. Acta* **75**, 7146–7179.
- Monterio F. M., Pancost R. D., Ridgwell A. and Donnadieu Y. (2012) Nutrients as the dominant control on the spread of anoxia and euxinia across the Cenomanian-Turonian oceanic anoxic event [OAE2]: model-data comparison. *Paleoceanography* **27**, PA4209. <http://dx.doi.org/10.1029/2012PA002351>.
- Nägler T. F. et al. (2011) Molybdenum isotope fractionation in pelagic euxinia: evidence from the modern Black and Baltic Seas. *Chem. Geol.* **289**, 1–11.
- Nägler T. F. et al. (2014) Proposal for an international molybdenum isotope measurement standard and data representation. *Geostand. Geoanal. Res.* **38**, 149–151.
- Neubert N., Nägler T. F. and Böttcher M. E. (2008) Sulphidity controls molybdenum isotope fractionation into euxinic sediments: evidence from the modern Black Sea. *Geology* **36**, 775–778.
- Neubert N. et al. (2011) The molybdenum isotopic composition in river water: constraints from small catchments. *Earth Planet. Sci. Lett.* **304**, 180–190.
- Owens J. D. et al. (2013) Sulfur isotopes track the global extent and dynamics of euxinia during Cretaceous Oceanic Anoxic Event 2. *PNAS* **110**, 18407–18412.
- Pancost R. D. et al. (2004) Further evidence for the development of photic-zone euxinic conditions during Mesozoic oceanic anoxic events. *J. Geol. Soc. London* **161**, 353–364.
- Parente M., Frijia G. and Di Lucia M. (2007) Carbon-isotope stratigraphy of Cenomanian-Turonian platform carbonates from the southern Apennines (Italy): a chemostratigraphic approach to the problem of correlation between shallow-water and deep-water successions. *J. Geol. Soc.* **164**, 609–620.
- Pearce C. R., Cohen A. S., Coe A. L. and Burton K. W. (2008) Molybdenum isotope evidence for global ocean anoxia coupled with perturbations to the carbon cycle during the Early Jurassic. *Geology* **36**, 231–234.
- Pearce C. R., Cohen A. S. and Parkinson I. J. (2009) Quantitative separation of Molybdenum and Rhenium from geological materials for isotopic determination by MC-ICP-MS. *Geostand. Geoanal. Res.* **33**(2), 219–229.
- Pearce C. R., Burton K. W., Pogge van Strandmann P. A. E., James R. H. and Gíslason S. R. (2010) Molybdenum isotope behaviors accompanying weathering and riverine transport in a basaltic terrain. *Earth Planet. Sci. Lett.* **295**, 104–114.
- Pogge van Strandmann P. A. E., Jenkyns H. C. and Woodfine R. G. (2013) Lithium isotope evidence for enhanced weathering during Oceanic Anoxic Event 2. *Nat. Geosci.* **6**, 668–672.
- Poulson-Brucker R. L., McManus J., Severmann S. and Berelson W. M. (2009) Molybdenum behavior during early diagenesis:

- insights from Mo isotopes. *Geochemist., Geophys. Geosyst.* **10**, Q06010. <http://dx.doi.org/10.1029/2008GC002180>.
- Poulson-Brucker R. L., McManus J. and Poulton S. W. (2012) Molybdenum isotope fractionations observed under anoxic experimental conditions. *Geochem. J.* **46**, 201–209.
- Poulson R. L., Siebert C., McManus J. and Berelson W. M. (2006) Authigenic molybdenum isotope signatures in marine sediments. *Geology* **34**, 617–620.
- Poulton S. W., Henkel S., März C., Urquhart H., Flögel S., Kasten S., Sinninghe Damsté J. S. and Wagner T. (2015) A continental-weathering control on orbitally driven redox-nutrient cycling during Cretaceous Oceanic Anoxic Event 2. *Geology*. <http://dx.doi.org/10.1130/G36837.1>.
- Rudnick, R.L. and S. Gao (2003) Composition of the continental crust. In *Treatise on Geochemistry* (eds D.H. Heinrich and K.T. Karl). Pergamon, Oxford, U.K, pp. 1–64.
- Sageman B. B., Meyers S. R. and Arthur M. A. (2006) Orbital time scale and new C-isotope record for the Cenomanian-Turonian boundary stratotype. *Geology* **34**, 125–128.
- Schlanger, S.O., Arthur, M.A., Jenkyns, H.C. and Scholle, P.A. (1987) The Cenomanian–Turonian Oceanic Anoxic Event, I. Stratigraphy and distribution of organic carbon-rich beds and the marine  $\delta^{13}\text{C}$  excursion. *Marine Petroleum Source Rocks* (eds Brooks, J. Fleet, A.J.). Geol. Soc. Lon. Sp. Pub. 26, 371–399.
- Schlanger S. O. and Jenkyns H. C. (1976) Cretaceous oceanic anoxic events: causes and consequences. *Geol. Mijnbouw* **55**, 179–184.
- Scott C. et al. (2008) Tracing the stepwise oxygenation of the Proterozoic ocean. *Nature* **452**, 456–459.
- Scott C. and Lyons T. W. (2012) Contrasting molybdenum cycling and isotopic properties in euxinic versus non-euxinic sediments and sedimentary rocks: refining the paleoproxies. *Chem. Geol.* **324–325**, 19–27.
- Siebert C., Nägler T. F., von Blanckenburg F. and Kramers J. D. (2003) Molybdenum isotope records as a potential new proxy for paleoceanography. *Earth Planet. Sci. Lett.* **211**, 159–171.
- Sinninghe Damsté J. S. and Koster J. (1998) A euxinic southern North Atlantic Ocean during the Cenomanian/Turonian oceanic anoxic event. *Earth Planet. Sci. Lett.* **158**, 165–173.
- Sinninghe Damsté J. S., Kuypers M. M. M., Pancost R. D. and Schouten S. (2008) The carbon isotopic response of algae, (cyano)bacteria, archaea and higher plants to the late Cenomanian perturbation of the global carbon cycle: Insights from biomarkers in black shales from the Cape Verde Basin (DSDP Site 367). *Org. Geochem.* **39**, 1703–1718.
- Takashima R. et al. (2011) Prevailing oxic environments in the Pacific Ocean during the mid-Cretaceous Oceanic Anoxic Event 2. *Nat. Commun.* **2**. <http://dx.doi.org/10.1038/ncomms1233>.
- Tossell J. A. (2005) Calculating the partitioning of the isotopes of Mo between oxidic and sulfidic species in aqueous solution. *Geochim. Cosmochim. Acta* **69**, 2981–2993.
- Trabucho Alexandre J. et al. (2010) The mid-Cretaceous North Atlantic nutrient trap: black shales and OAEs. *Paleoceanography* **25**, PA4201. <http://dx.doi.org/10.1029/2010PA001925>.
- Tribouillard N., Algeo T. J., Lyons T. and Riboulleau A. (2006) Trace metals as paleoredox and paleoproductivity proxies: an update. *Chem. Geol.* **232**, 12–32.
- Tsikos H. et al. (2004) Carbon isotope stratigraphy recorded by the Cenomanian-Turonian Oceanic Anoxic Event: correlation and implications based on three key localities. *J. Geol. Soc. London* **161**, 711–719.
- Turgeon S. C. and Creaser R. A. (2008) Cretaceous oceanic anoxic event 2 triggered by a massive magmatic episode. *Nature* **454**, 323–326.
- van Bentum E. C., Reichart G.-J. and Sinninghe-Damsté J. S. (2012) Organic matter provenance, paleoproductivity and bottom water anoxia during the Cenomanian/Turonian oceanic anoxic event in the Newfoundland Basin [northern proto North Atlantic Ocean]. *Org. Geochem.* **50**, 11–18.
- Voigt et al. (2008) The Cenomanian-Turonian of the Wunstorf section – (North Germany): global stratigraphic reference section and new orbital time scale for Oceanic Anoxic Event 2. *News. Stratigr.* **43**(1), 65–89.
- Wasylenki L. E., Rolfe B. A., Weeks C. L., Spiro T. G. and Anbar A. D. (2008) Experimental investigation of the effects of temperature and ionic strength on Mo isotope fractionation during adsorption to manganese oxides. *Geochim. Cosmochim. Acta* **72**(24), 5997–6005.
- Wen H., Carignan J., Cloquet C., Zhu X. and Zhang Y. (2010) Isotopic delta values of molybdenum standard reference and prepared solution measured by MC-ICP-MS: proposition for delta zero and secondary references. *J. Anal. Atom. Spec.* **25**, 716–721.
- Westermann S., Caron M., Fiet N., Fleitmann D., Matera V., Adatte T. and Föllmi K. B. (2010) Evidence for oxic conditions during oceanic anoxic event 2 in the northern Tethyan pelagic realm. *Cretaceous Res.* **31**, 500–514.
- Westermann S., Vance D., Cameron V., Archer C. and Robinson S. A. (2014) Heterogeneous oxygenation states in the Atlantic and Tethys oceans during Oceanic Anoxic Event 2. *Earth Planet. Sci. Lett.* **404**, 178–189.
- Wiese, F. (2009) The Söhlde Formation (Cenomanian, Turonian) of NW Germany: shallow marine pelagic red beds. In: *Cretaceous Oceanic Red Beds: Stratigraphy, Composition, Origins, and Paleoclimatic and Palaeoclimatic Significance, SEPM Special Publication*, vol. 91, pp. 153–170.
- Zheng X.-Y., Jenkyns H. C., Gale A. S., Ward D. J. and Henderson G. M. (2013) Changing ocean circulation and hydrothermal inputs during Ocean Anoxic Event 2 (Cenomanian–Turonian): evidence from Nd-isotopes in the European shelf sea. *Earth Planet. Sci. Lett.* **375**, 338–348.

Associate editor: Timothy Lyons